RSC Advances

ROYAL SOCIETY OF CHEMISTRY

www.rsc.org/advances

Effective removal of Cr(VI) through adsorption and reduction by magnetic mesoporous carbon incorporated with polyaniline

Guide Yang [a, b], Lin Tang [a, b,*], Ye Cai [a, b], Guangming Zeng [a, b,*], Pucan Guo [a, b], Guiqiu Chen [a, b], Yaoyu Zhou [a, b], Jing Tang [a, b], Jun Chen [a, b], Weiping Xiong [a, b]

[a] College of Environmental Science and Engineering, Hunan University, Changsha, 410082, PR China

[b] Key Laboratory of Environmental Biology and Pollution Control, Hunan University, Ministry of Education, Changsha 410082, PR China

*Corresponding author: E–mail: tanglin@hnu.edu.cn (Lin Tang), zgming@hnu.edu.cn (Guangming Zeng)

Tel.: +86–731–88822778; Fax: +86–731–88822778.

Abstract

Magnetic mesoporous carbon incorporated with polyaniline (PANI–Fe/OMC) was developed for enhanced adsorption and reduction of toxic Cr(VI) to non–toxic Cr(III). Several physicochemical techniques including TEM, FTIR and XPS analyses confirmed that magnetic iron nanoparticles and amino groups have been successfully bound on the mesoporous matrix. The adsorption capacity of the functionalized material is two- and ten- folds of the magnetic mesoporous carbon (Fe/OMC) and pristine mesoporous silicon (SBA-15), respectively. Solution pH exhibited a remarkable impact on the Cr(VI) adsorption and the maximum uptake amount (172.33 mg/g) occurred at pH 2.0. The well fitting of adsorption process using pseudo–second–order and Langmuir models indicated the chemisorption process of Cr(VI) removal. The regeneration study revealed that PANI–Fe/OMC can be reused without loss of their activity in repetitive adsorption tests. Moreover, the resultant adsorbent can be effectively applied in actual wastewater treatment due to the excellent removal performance in fixed–bed column and real water samples. The interaction between Cr(VI) and PANI–Fe/OMC was investigated by FTIR and XPS analyses. The results indicated that the amino groups on the surface of PANI–Fe/OMC are involved in Cr(VI) uptake, and simultaneously some toxic Cr(VI) were reduced to non–toxic Cr(III) during the removal process.

1. Introduction

Chromium is a common contaminant in surface water and groundwater due to its widespread use in many industrial activities such as electroplating, leather tanning, pigmentation, and etc.[1] Depending on the pH levels, chromium most frequently occurs in two common oxidation states in wastewater: hexavalent chromium (Cr(VI)) and trivalent chromium (Cr(III)). Cr(III) is harmfulless and immobile in aqueous media, however Cr(VI) is highly toxic, carcinogenic and mutagenic to all forms of living organisms.[2,3] The maximum permissible limit of Cr(VI) for industrial effluents to be discharged to surface water in China is 50 μg/L.[4] Consequently, it is indispensable to develop an economical, effective and reliable water treatment technique to remediate Cr(VI) contamination from water.

Conventional remediation techniques, including electrochemical precipitation, redox treatments, biological processes and ion exchange have been proposed to remediate Cr(VI)–contaminated wastewaters. Of these, chemical precipitation is considered to be the most promising and economical method. This technique, however, produces large amounts of precipitate sludge that requires additional process for the further treatment.[5] Although redox is maneuverable and easy to implement, it needs continual energy and reagents supply.[6] Biological processes, on the other hand, exhibit a low efficiency and long operation time for effective treatment to be achieved.[7] Ion exchange is a simple approach to treat the contaminated water, but only limited literatures have been reported on the removal of Cr(VI). In addition, the relevant cost is higher than that of other methods as well.[8] By contrast, remediation of Cr(VI) contamination through adsorption is a promising technique because of its low

cost, ambient conditions, high efficiency and simple operation.[9-11] Various adsorbents include activated carbons,[12] clays,[13] chitosan,[14] and polymeric resins[10] have been applied for elimination of Cr(VI) in wastewater. However, several problems, including low adsorption capacity, slow process kinetics and poor mechanical strength turn out to be the huge flaws, which affect seriously these adsorbents practical application.

Recently, mesoporous materials have been widely investigated as promising candidates for various organic matters and metal ions removal because of their large pore volumes, high surface areas and excellent physical–chemical properties.[15,16] However, the large–scale application of mesoporous adsorbents is a challenge due to the costly separation process. Magnetic separation has been proved to be an attractive technique for the fast separation rate, high efficiency, and simply and conveniently experimental manipulation.[17,18] As a consequence, magnetic mesoporous adsorbent, as an excellent functional remediation material, has aroused increasing interests around the world. Polyaniline (PANI) is one of the most extensively used and studied conducting polymers. Because of its mechanical flexibility, environmental stability, easy synthesis and in–built amino groups, PANI has great application advantages in wastewater treatment. The polymer not only can efficiently chelate with toxic Cr(VI) through electrostatic interaction, but also reduce fractional Cr(VI) to low toxicity of Cr(III).[19,20] However, the regenerate and reuse of PANI is a large challenge due to the small size of raw PANI. Therefore, it is requisite to incorporate PANI into support materials to overcome the disadvantages. To our best knowledge, only synthesis of

PANI modified mesoporous carbon has been attempted, while research on preparation of functional mesoporous adsorbent combining the multiple advantages of mesoporous carbon, magnetic nanoparticles and PANI, as well as its excellent behaviors for Cr(VI) removal has not been reported.

In this study, a novel functional adsorbent, magnetic mesoporous carbon incorporated with PANI, was prepared by in–situ polymerization of aniline onto magnetic mesoporous carbon matrix. After systematic characterization of its structural properties, the resultant remediation material was applied for removal of Cr(VI) from water. Batch and fixed–bed experiments were used to investigate the adsorption behaviors of Cr(VI), and the kinetics, isotherms and thermodynamics were also utilized to evaluate the relevant Cr(VI) removal mechanisms. The effect of co–existing interferences and the regeneration of PANI–Fe/OMC were examined for its actual application. The interaction mechanisms between Cr(VI) and the modified mesoporous carbon were further explored.

2. Methods and materials

2.1. Prepared of PANI–Fe/OMC

Pluronic copolymer P123 ($EO_{20}PO_{70}EO_{20}$) was obtained from Sigma–Aldrich (USA). Solid humic acid (HA, (50–60% purity) was purchased from Acros Organics (Belgium) and solid fulvic acid (FA, 70% purity) was purchased from Shijiazhuang Lemandou Chemicals Co., Ltd. (China). The main elements of HA are: C 60.44%, H 3.53%, N4.22%,O31.31% and S 0.50%; and those of FA are: C50.55%, H 4.12%, N 5.28%, O 39.56% and S 0.49%. Cross-polarization magic angle spinning ^{13}CNMR

spectra of HA and FA were divided into four chemical shift regions: 0–50 ppm, 51–105 ppm, 106–160 ppm and 161–200 ppm. These regions were referred to as aliphatic, carbohydrate, aromatic and carboxyl regions. All other chemicals used were of analytical grade and were used without further purification. Aniline was distilled under vacuum before use. Stock solution of 1000 mg/L Cr(VI) was prepared from $K_2Cr_2O_7$. All stock solutions were prepared with high–purity water (18.25 MΩ cm, Milli–Q). Mesostructured SBA–15 silica template was prepared as follows according to literature,[21] and magnetic mesoporous carbon (Fe/OMC) was synthesized as described previously with slight alterations.[22]

Modified magnetic mesoporous nanocomposite was obtained by oxidative polymerization of aniline.[23] In specific, 2.0 mL of aniline was added into 400 mL of 0.2 M HCl solution, and then 1.0 g of Fe/OMC was added slowly under mechanical stirring. Following on it, ammonium persulfate (APS) with a molar ratio of aniline/APS of 1:1 was dissolved into 100 mL of 0.2 M HCl solution before putting into the above mixed solution. The in–situ polymerization was carried out in an ice–water bath for 12 h continuous stirring. Then, the resultant solid was collected by magnetic separation and washed with high–purity water and ethanol for several times. Finally, the desired product was obtained by drying in vacuum at 333 K overnight. Details about the preparation of SBA–15 and Fe/OMC were presented in Supporting Information (SI).

2.2 Materials Characterization

The synthesized samples were characterized before and after chemical modification by Transmission electron microscopy (TEM), Brunauer–Emmett–Teller (BET) and Barrett–Joyner–Halenda (BJH) methods, Fourier transform–infrared techniques (FTIR), X–ray photoelectron spectra (XPS) and Zeta potential measurements. TEM images were obtained on a JEOL–1230 electron microscope operated at 100 kV (Dot resolution: 0.24 nm and angle of inclination: $\pm 20^{\circ}$). FTIR spectra were recorded with a Nicolet NEXUS 670 FTIR spectrometer by the standard KBr disk method. XPS analyses were conducted on an X–ray photoelectron spectroscopy (Thermo Fisher Scientific, UK) with a resolution of 0.5 eV. BET and BJH measurements were carried out by a Micromeritics 2020 analyzer at 77 K. Zeta potential measurements versus pH have been collected using a Malvern ZEN3600 Zetasizer Nano.

2.3 Batch adsorption experiments and chemical analysis

Batch adsorption experiments of Cr(VI) were performed in duplicate in 50–mL sealed conical flasks on a shaker at 150 rpm. The pH of the suspension was adjusted by 0.1 M NaOH or HNO_3 solution. In each procedure, 10 mg of the PANI–Fe/OMC was added into 10 mL of Cr(VI) solution in desired concentration (10-500 mg/L) at pH 2.0. After the suspension was reacted for 3 h to reach equilibrium, the used adsorbent was separated by applying an external magnetic field for 3 min. The initial and residual concentrations of Cr(VI) in the supernatants was analyzed using the 1,5–diphenylcarbazide method with a UV–vis spectrophotometer (UV–754N shanghai, China) at wavelength of 540 nm, and the corresponding total Cr was

146 determined by a Perkin–Elmer Analyst 700 atomic absorption spectrophotometer
147 (AAS, Perkin–Elmer, USA).

148 The adsorption capacity and the adsorption efficiency of PANI–Fe/OMC were
149 calculated according to the following equations:

150 $$q_e = \frac{(C_0 - C_e) \times V}{W} \quad (1)$$

151 $$R(\%) = \frac{C_0 - C_e}{C_0} \times 100 \quad (2)$$

152 where q_e is the adsorption capacity of PANI-Fe/OMC towards Cr(VI) (or total Cr)
153 (mg/g); C_0 and C_e are the initial and residual concentration of Cr(VI) (or total Cr) in
154 solution (mg/L), respectively; V is the volume of the suspension (mL), W is the mass
155 of adsorbent used (mg) and R(%) is the adsorption efficiency.

156 The effect of different interferences on Cr(VI) adsorption was conducted in this
157 study. Specifically, 10 mg of the PANI–Fe/OMC was added into 10 mL of the
158 solution containing 80mg/L of Cr(VI) and desired concentrations of the interferents
159 (Cl^-, NO_3^-, SO_4^{2-}, PO_4^{3-} HA or FA) (10-500mg/L). After 3 h of reaction, the residual
160 Cr(VI) was analyzed by AAS.

161 The regeneration studies of PANI–Fe/OMC were carried out in the batch process.
162 Typically, 10 mL of 80 mg/L Cr(VI) solution was adsorbed first by 10 mg of
163 PANI–Fe/OMC for 3 h to reach adsorption equilibrium. The used PANI–Fe/OMC
164 was separated magnetically from the suspension and then washed thoroughly with
165 ultrapure water to neutrality before desorbing with 10 mL of 0.1 M NaOH solution for
166 24 h. After magnetic separation and drying at 333 K overnight, the regenerative
167 adsorbent was again used in the succeeding cycle.

2.5 **Fixed–bed column experiments**

Fixed–bed column tests were carried out at 298 K in three small polyethylene columns (10 mm diameter and 200 mm length). 1.0 g of SBA–15, Fe/OMC or PANI–Fe/OMC was put into each column, respectively. Then, the Cr(VI) solution with the initial concentration of 80 mg/L at pH 2.0 was pumped into per column in a down–flow direction using a peristaltic pump at the desired flow rate of 8 mL/min. The effluent samples were collected and the residual Cr(VI) was analyzed by the above UV–vis spectrophotometer.

3. Results and discussion

3.1 Characterization of PANI–Fe/OMC

The mesoporous structures of SBA–15 and PANI–Fe/OMC were characterized by the TEM technique (Fig. 1). Representative highly aligned stripe–like and hexagonally arranged structure with cylindrical pores was clearly observed, demonstrating that the resultant mesoporous materials possesses well ordered 2D hexagonal mesostructures.[24] The black nanoparticles dispersed uniformly on the carbon matrix were magnetic iron particles. The isotherm curves of the as–synthesized nanoparticles (Fig. S1) shows typical type IV curves with broad capillary condensation steps at the relative pressure (P/P_0) of 0.4−0.8, indicating a narrow pore size distribution with uniform mesopores, which is further confirmed by the pore–size distribution profile from adsorption curve (Fig. S1 insert). After the functionalization, decreases in surface area (374.89−55.95 m^2/g) and pore volume (0.60−0.11 cm^3/g) are distinctly observed (Table S1). However, the pore diameter

decreases slightly (4.81−4.74 nm), which is probably related with that the functional groups are preferentially grafted near the pore entrances.[25]

The chemical compositions of mesoporous materials were characterized by FTIR technique (Fig. 2). The functional groups of the modified mesoporous material are significantly distinctive with those of the pristine mesoporous materials. Specifically, the strong peak around 3560 cm^{-1} corresponds to N−H stretching, and the two main bands at 1475 and 1592 cm^{-1} are related to the C=C stretching vibration modes of benzenoid and quinoid rings of PANI, corresponding to the extent of reduction and oxidation of PANI, respectively.[23] And meanwhile, the two C=C stretching vibration peaks also indicate that the resultant polyaniline is functionalized in the emeraldine salt form, capable of being further oxidized and reduced.[19] The peaks at 1302 and 1140 cm^{-1} can be assigned to C–N stretching and C–H in–plane bending of pernigraniline, respectively.[26] The weak adsorption peak at 567 cm^{-1} is attributed to the Fe–O stretch vibration.[27] The survey XPS spectrum of the PANI–Fe/OMC is shown in Fig. S2a and b. As expected, all the peaks assigned for carbon (C1s), nitrogen (N1s), iron (Fe 2p3) and oxygen (O1s) can be clearly seen (Table S2). After contact with Cr(VI), chromium (Cr 2p3) is also present in the spectrum (Fig. S2b). The FTIR and XPS analyses have confirmed that PANI has been successfully polymerized on the masoporous matrix.

Zeta potentials of both mesoporous materials were measured in a wide range of pH (from 2 to 11) and the corresponding results were presented in Fig. S3. The isoelectric points (pH_{ZPC}) of the magnetic mesoporous material increased from 4.8 to

10.0 or so after incorporation with PANI. The enhanced isoelectric points of PANI–Fe/OMC could yield stronger electrostatic attraction between nanoparticles and Cr(VI) anions, and thus the chromium uptake efficiencies would increase.

3.2 Adsorption kinetics

Adsorption of Cr(VI) on three different mesoporous adsorbents as a function of contact time is presented in Fig. 3a. As seen, the Cr(VI) adsorption on PANI–Fe/OMC exhibited an initial rapid adsorption followed by a slow removal rate that gradually reached equilibrium. Adsorption equilibrium was reached within 120 min, and the equilibrium adsorption efficiency of PANI–Fe/OMC arrived 92%, which was approximately two– and ten– folds as high as that of Fe/OMC and SBA–15, respectively. Since the specific surface area of PANI–Fe/OMC was 55.95 m^2/g, smaller than Fe/OMC (374.89 m^2/g) and SBA–15 (575.21 m^2/g), the micropore adsorption of Cr(VI) was negligible, and the excellent adsorption behavior by PANI–Fe/OMC was probably related with the introduction of amine groups. Large number of amine groups on the PANI–Fe/OMC surface offered additional affinity and more available binding sites for Cr(VI), accelerating the uptake of Cr(VI). The spectrophotometric techniques were used to characterize the Cr(VI) adsorption process, the Cr(VI) showed a characteristic peak at 350 nm in the UV–vis absorption curve (Fig. 3b).[28] The peak gradually slowed down with time from 0 to 180 min, and it could reflect well the adsorption behavior of PANI–Fe/OMC. To make certain the adsorption process, two kinetic models, the pseudo–first–order and the pseudo second–order models were used to describe the kinetics of Cr(VI) adsorption. The

234 relevant equations of Eq. (3) (pseudo–first–order model) and Eq. (4)
235 (pseudo–second–order model) are as follows:

236 $$\frac{dq_t}{dt} = k_1(q_e - q_t) \quad (3)$$

237 $$\frac{dq_t}{dt} = k_1(q_e - q_t)^2 \quad (4)$$

238 where q_e and q_t (mg/g) are the adsorption capacities of PANI-Fe/OMC at equilibrium
239 and time t (min), respectively, k_1 (min^{-1}) and k_2 (g/mg·min) are the related rate
240 constants, respectively. The fit of pseudo–second–order model was presented in the
241 inset of Fig. 3a, and the corresponding two model parameters were listed in Table 1.
242 As seen, the pseudo–second–order model could better fit the adsorption process with
243 a higher correlation coefficient ($R^2 > 0.99$), suggesting that the Cr(VI) adsorption was
244 involved in the chemisorption rate–controlling mechanism.[29]

245 **3.3 Effect of pH**

246 Fig. 4a shows Cr(VI) adsorption on PANI–Fe/OMC as a function of pH in
247 different initial Cr(VI) concentrations at 298 K. It indicated that the adsorption
248 capacity declined with the increase of pH, and the maximum uptake amount attained
249 approximately 172 mg/g at pH 2.0. Compared with just over 79 mg/g of uptake
250 amount at pH 9.0, the solution pH demonstrated a significantly effect on Cr(VI)
251 removal. This phenomenon is related with the surface property of the mesoporous
252 adsorbent. Since the pH_{ZPC} of PANI–Fe/OMC is around 10.0, the surface charge of
253 the PANI–Fe/OMC at pH< pH_{ZPC} is positive due to the protonation reaction.
254 Obviously, lower pH can lead to more positive charge on the surface of the adsorbent,

and thus anionic species of Cr(VI), such as $Cr_2O_7^{2-}$, CrO_4^{2-}, and $HCrO_4^-$, can easily be adsorbed onto the PANI–Fe/OMC surface because of electrostatic attraction.[10] The Eq. (5)–(6) indicates the protonation of the amino groups in PANI–Fe/OMC and the reaction between the protonated adsorbent and Cr(VI). With pH increase, the available positively charged adsorption sites decreased gradually; consequently, only a handful of Cr(VI) could be removed by the nanoparticles.

$$R–NH_2+H^+ \rightarrow R–NH_3^+ \quad (5)$$

$$2R–NH_3^+ + Cr_2O_7^{2-} \rightarrow R–NH_3^+ – Cr_2O_7^{2-} – {}^+{}_3HN\text{-}R \quad (6)$$

Isothermal adsorption is a requisite to expound the adsorption process. In the study, two typical isotherm adsorption models, Langmuir and Freundlich isotherm models are applied to fit the isothermal adsorption data. The relevant equations are expressed in Eq. (7)–(8):

$$q_e = \frac{q_{\max} K_L C_e}{1 + K_L C_e} \quad (7)$$

$$q_e = K_F C_e^{1/n} \quad (8)$$

where q_{max} (mg/g) is the maximum amount of adsorption corresponding to complete monolayer coverage, q_e (mg/g) and C_e are the equilibrium adsorption capacity and equilibrium Cr(VI) concentration, K_L (L/mg) is the Langmuir constant related to adsorption energy, K_F is the Freundlich related to the sorption capacity, and n is the constant representing adsorption intensity. The adsorption isotherm was represented in Fig. 4a and the relevant parameters calculated from the Langmuir and Freundlich isotherm models were listed in Table 2. It was noticeable that the Langmuir model with a correlation of over 0.98 gave a better fit to the equilibrium data. The results are

in agreement with previous studies for Cr(VI) adsorption,[9,30] and it assumed that the adsorption of Cr(VI) onto PANI–Fe/OMC was mainly chemisorption. A comparison has been made between the resultant PANI-Fe/OMC and previously reported adsorbents for Cr(VI) adsorption (Table 3). [19,30-38] The results of the analyses demonstrated that this novel functional adsorbent gain the advantage over many other adsorbents, indicating that PANI-Fe/OMC is a fairly promising candidate for treatment of chromium-containing wastewater.

In order to determine how Cr(VI) interacts with PANI–Fe/OMC, the total chromium concentration was measured at pH 2.0 and the result was shown in Fig. S4. The Cr(VI) removal distinguish obviously with the total Cr, indicating that the Cr(VI) was not entirely removed due to the adsorption, and simultaneously, a non–ignorable portion of Cr(VI) was reduced to Cr(III).[39] The Cr(VI) removal is an adsorption–couple reduction process.

3.4 Thermodynamic of adsorption

Fig. 4b shows the effect of temperature on Cr(VI) adsorption onto the PANI–Fe/OMC at pH 2.0. The adsorption isotherms of Cr(VI) onto the modified mesoporous adsorbent at different temperatures were also listed in Table 2. The adsorption capacity of PANI–Fe/OMC increased from 151.60 mg/g to 204.56 mg/g with temperature increase from 283 K to 303 K, which demonstrated that the Cr(VI) adsorption was better at higher temperatures.[40] Additionally, thermodynamic parameters such as free energy change (ΔG), enthalpy change (ΔH) and entropy

change (ΔS) were exploited to explore the further interaction, and the relative thermodynamics equations are expressed as follows:

$$\ln K_L = \frac{\Delta S}{R} - \frac{\Delta H}{RT} \quad (9)$$

$$\Delta G = \Delta H - T\Delta S \quad (10)$$

where K_L is the Langmuir constants (L/mol), R is the ideal gas constant (8.314 J/mol/K) and T is the absolute temperature (K). ΔH and ΔS are calculated from the slope and intercept of the linear plots of lnK_L versus 1/T. The ΔG, ΔH, and ΔS values are listed in Table 4. The negative ΔG values indicate that the Cr(VI) uptake process were thermodynamically feasible and spontaneous under the experimental conditions.[41] The positive value of ΔH^0 (10.45 kJ/mol) for Cr(VI) adsorption confirmed the endothermic nature of adsorption, and the positive value of ΔS^0 (109.42 J/mol/K) suggests an increased randomness occurring at the solid solution interface during the adsorption process.

3.5 Effect of co–existing interferents

In natural environment, Cr(VI) often co–exists with other inorganic and organic substances, which may compete for adsorption sites and decrease the Cr(VI) removal efficiency of the PANI–Fe/OMC. Based on this, the effect of commonly co–existing interferents is investigated in this study.

3.5.1 Inorganic interferents

Fig. 5 presented the effect of common anions on Cr(VI) adsorption with the initial Cr(VI) concentration of 80 mg/L at 298 K. As the additional interferents concentrations increased, the Cr(VI) removal capacity almost remain steady in the

solution containing monovalent Cl^- or NO_3^- anion, while it exhibited a slight decrease under divalent SO_4^{2-} or trivalent PO_4^{3-} anion. This is because compared with monovalent Cl^- and NO_3^- anions, the physicochemical properties of SO_4^{2-} and PO_4^{3-} anions are more similar to Cr(VI) oxyanions, that is, with almost equivalent ion sizes and structures,[9] and thus these anions may compete with Cr(VI) for available adsorption sites of adsorbents. Thus, SO_4^{2-} and PO_4^{3-} anions are more influential than Cl^- and NO_3^- anions. Given the lower limited concentrations of SO_4^{2-} and PO_4^{3-} in natural water (0–5 mg/L),[42] the interference from sulphate and phosphate were almost insignificant.

3.5.2 Organic interferents

The effect of co–existing organic substances on the adsorption of Cr(VI) are investigated in the inset of Fig. 5. The existence of the two organic interferents, HA and FA, can accelerate Cr(VI) adsorption at lower concentrations, while an obvious suppression occurs at higher interferent concentrations. The promotion impact suggests HA and FA may act as a scavenger for the uptake of Cr(VI). On one hand, large amounts of Cr(VI) were adsorbed on the PANI–Fe/OMC surface, and on the other hand, HA and FA were firstly adsorbed onto the original adsorption sites on the PANI–Fe/OMC surface, and then the fraction of the residual Cr(VI) interacted with the new adsorption sites caused by HA and FA adsorption.[43] Thus, the Cr(VI) removal amount was enhanced under lower HA and FA concentrations. While at higher HA and FA concentrations, these extra additives might compete with Cr(VI)

for the adsorption sites on the resultant sample, such as amine groups, thus resulting in a decrease in the uptake of Cr(VI).

3.6 Regeneration of PANI-Fe/OMC

Regeneration and reuse tests were conducted to regenerate used PANI–Fe/OMC using 0.1 M NaOH in Fig. S5. The result demonstrated the adsorption activity of PANI–Fe/OMC deteriorated with the increase in the number of reuse cycle, but only very slight. The adsorption efficiency could still reach 90% in the seventh reuse cycle, which demonstrated that PANI–Fe/OMC was capable of being regenerated and reused effectively.

3.7 Fixed–bed column adsorption

Column studies were used to examine the performance of the three adsorbents to remove Cr(VI) from water (Fig. 6a). As expected, the uptake of Cr(VI) through SBA–15 and Fe/OMC columns showed the poor performance, and the saturation adsorption capacities of Cr(VI) were only less than 240 and 640 bed volumes (BV), respectively, much less than that of PANI–Fe/OMC with 1300 BV of saturation sorption amount. Furthermore, three different real water environments, including ultrapure water, tap water and river water were used to evaluate the adsorption behavior of PANI–Fe/OMC (Fig. 6b). It indicated that the uptake capacities of Cr(VI) were slightly limited in tap water whereas an acceleration in river water than ultrapure water. The distinct performance might be related to different co–existing substances, such as sulfate ions and phosphate ions in tap water and some common organics in

river water.[41] As above mentioned, these interferents could suppress or boost the uptake of Cr(VI) to some extent, respectively.

3.8 Removal mechanism

Given that the surface areas of PANI–Fe/OMC smaller than Fe/OMC and SBA–15, the simple physic adsorption through intraparticle diffusion was eliminated, and the significant improvement in Cr(VI) uptake onto PANI–Fe/OMC is probably related with the chemical interaction at the solid/liquid interface. To gain further insights into the uptake mechanism of Cr(VI) on PANI–Fe/OMC, FTIR technique was used to analyzed the exhausted PANI–Fe/OMC. As shown in Fig. 7, the FTIR spectrum of PANI–Fe/OMC underwent several substantial changes after Cr(VI) adsorption. The increase in the peak at 1592 cm^{-1} indicates that the oxidation extent of PANI was amplified after the uptake of Cr(VI).[44] The decrease in absorption intensity at 1475 cm^{-1} suggests that some benzenoid amines of PANI have been oxidized from the emeraldine salt form to the pernigraniline form (quinoid amine, the highest oxidation state of PANI) during the Cr(VI) removal process.[45] The relative absorption intensity at 882 cm^{-1} for the used PANI–Fe/OMC was attributed to Cr–O mode, weaker than the characteristic infrared band of free chromate (890 cm^{-1}), which may be related to hydrogen bonding of the $HCrO_4^-$ with interlayer water molecules or layer hydroxyl groups.

Moreover, XPS spectra of PANI–Fe/OMC surfaces before and after Cr(VI) interaction were studied to elaborate the uptake process of Cr(VI). The chromium region is been determined by XPS and the results were shown in Fig. 8a and b. After

interaction with Cr(VI), the binding energies at 576.4 and 578.6 eV can be assigned to Cr(III) and Cr(VI), respectively. This suggests that both Cr(VI) and Cr(III) coexist on the surface of Cr(VI)–adsorbed PANI–Fe/OMC. High–resolution spectra of N1s showed that before Cr(VI) uptake, N1s region showed two distinct peaks at 398.3 and 399.2 eV, corresponding to nitrogen atoms in quinoid amine (–N=) and beneznoid amine (N–H), respectively (Fig. 8c).[46] After reaction with Cr(VI), the reduced nitrogen (N–H) sharply decreased from 11.05% to 5.02%, while a corresponding increase in oxidated nitrogen (–N=) from 88.95% to 91.76% (Fig. 8d). This further demonstrated the redox reaction occurring between Cr(VI) and the nitrogen atoms of PANI functional groups. Meanwhile, a new peak occurred at 401.2 eV, corresponding to nitrogen atoms in doped imine ($–N^{+}=$). This was probably due to the sharing of electrons between nitrogen atoms and chromium, which confirmed the fixation of Cr(VI) and chelation of Cr(III) onto the PANI–Fe/OMC. The O1s spectra of the PANI–Fe/OMC before and after interaction with Cr(VI) were shown in Fig. 8e and f. The broad peak of O1s could be fitted by three peaks at binding energies of 530.8, 532.2 and 533.3 eV, assigning to the oxygen atoms in O=C, O–C and O–H bonds, respectively.[47] After Cr(VI) adsorption, a non–ignorable binding energy at 532.7 eV could be assigned oxygen in the Cr–O bond, which indicated that oxygen atoms also participate in the chelation of Cr(III). The C1s and Fe2p spectra of the PANI–Fe/OMC before and after interaction with Cr(VI) were shown in Fig. S2c–f. The C1s spectra (Fig. S2c and d) were considered in the forms of C–C (283.7 eV), C–N (285.2 eV), and C–O (286.8 eV), respectively. The Fe2p spectra (Fig. S2e and f)

406 were in the forms of FeO (709.6 eV) and Fe_2O_3 (711.2 eV). As seen, no significant
407 changes were observed in the two spectra before and after interaction with Cr(VI),
408 indicating that carbon and iron atoms did not involve to the uptake of Cr(VI).

409 On the basis of the above analyses, the main reaction proceeding between Cr(VI)
410 and the PANI–Fe/OMC can be proposed in Fig. 9. First, the amine groups on the
411 adsorbent are protonated under the acidic conditions, and thus the surface
412 complexation occurred between protonated functional groups and aqueous Cr(VI)
413 oxyanions via electrostatic attraction. Then, because of its strong oxidation ability, the
414 adsorbed Cr(VI) can react with some reduction state of PANI compositions
415 (benzenoid amines) with an assistance of hydrogen ions. The result is that the
416 benzenoid amines are oxidated to quinoid amine, the highest oxidation state of PANI,
417 and some Cr(VI) oxyanions was reduced to Cr(III) cations. Finally, partial Cr(III)
418 cations were strongly fixed with the oxidated quinoid amines of PANI functional
419 groups.

420 **4. Conclusion**

421 In summary, a novel adsorbent of PANI–Fe/OMC nanopariticle with magnetic
422 separability was synthesized for effectively removal of Cr(VI) from water. The
423 resultant nanoparticle demonstrated a high adsorption capacity and fast rate for Cr(VI)
424 removal. Kinetics demonstrated the adsorption capacity of PANI–Fe/OMC was
425 obviously improved up to 2– and 10–folds compared with SBA–15 and Fe/OMC. The
426 maximum adsorption capacity occurred at pH 2.0 and the adsorption data can be
427 better fitted by Langmuir model. Thermodynamics revealed that the Cr(VI)

adsorption was an endothermic and spontaneous nature process. Other common coexisting ions had limited influence on the adsorption capacity, while the coexisting organic interferents showed an acceleration and then suppression of Cr(VI) removal with the increase of initial concentrations of HA and FA. Fixed–bed column experiments demonstrated that modified magnetic mesoporous carbon had great superior over other mesoporous adsorbents and could be well applied in actual chromium contamination treatment. Regeneration and reuse indicated that PANI–Fe/OMC could be well regenerated and maintained at over 90% of Cr(VI) adsorption efficiency in the seventh cycles. Further investigation by the comparison of FTIR and XPS spectra before and after adsorption indicated that Cr(VI) removal by PANI–Fe/OMC was a adsorption–coupled reduction process for the existence of Cr(III) and the change of nitrogen atoms in functional groups. Results from this study demonstrate the resultant PANI–Fe/OMC nanopariticle can be used as a potential novel candidate for the removal of Cr(VI) from wastewater.

Acknowledgements

The study was financially supported by Program for the Young Top-Notch Talent Support Program of China (2012), the National Natural Science Foundation of China (51222805), the Program for New Century Excellent Talents in University from the Ministry of Education of China (NCET–11–0129), the Fundamental Research Funds for the Central Universities, Hunan University, China, and Foundation for the Author of Excellent Doctoral Dissertation of Hunan Province, China.

References

1. C. Kantar, Z. Cetin and H. Demiray, *J. Hazard. Mater.*, 2008, **159**, 287–293.

2. M. D. Nazime, K. Cetin, G. Sibel, J. D. Cleveland, C.Y. Banu and A.M. Mehmet, *Environ. Sci. Technol.*, 2011, **45**, 2278–2285.

3. S. Binoy, N. Ravi, S. K. Gummuluru and M. Mallavarapu, *Environ. Sci. Technol.*, 2013, **47 (23)**, 13629–13636.

4. Y. C. Zhang, J. Li, M. Zhang and D. D. Dionysiou, *Environ. Sci. Technol.*, 2011, **45**, 9324–9331.

5. D. Lin, S. Zhou, L. Bing, L. F. Yang, L. Lu and X. Z. Yang, *Ind. Eng. Chem. Res.*, 2014, **53 (18)**, 7746–7757.

6. L. Giehyeon, P. Jaeseon and R. H. Omar, *Water Res.*, 2013, **47**, 1136–1146.

7. X. H. Pan, Z. J. Liu, Z. Chen, Y. J. Cheng, D. M. Pan, J. N. Shao, Z. Lin and X. Guan, *Water Res.*, 2014, **55**, 21–29.

8. L. Alvarado, I. R. Torres and A. C. Chen, *Sep. Purif. Technol.* 2013, **105**, 55–62.

9. L. Tang, G. D. Yang, G. M. Zeng, Y. Cai, S. S. Li, Y. Y. Zhou, Y. Pang, Y. Y. Liu, Y. Zhang and B. Luna, *Chem. Eng. J.*, 2014, **239** 114–122.

10. X. F. Sun, Y. Ma, X. W. Liu, S. G. Wang, B. Y. Gao and X. M. Li, *Water Res.*, 2010, **44**, 2517−2524.

11. L. Y. Chai, Y. Y. Wang, N. Zhao, W. C. Yang and X. Y. You, *Water Res.*, 2013, **47**, 4040–4049.

12. Y. Y. Sun, Q. Y. Yue, B. Y. Gao, Y. Gao, Q. Li and Y. Wang, *Chem. Eng. J.*, 2013, **217**, 240–247.

13. Y. X. Zhao, S. J. Yang, D. H. Ding, J. Chen, Y. N. Yang, Z. F. Lei, C. P. Feng and Z. Y. Zhang, *J. Colloid Interf. Sci.*, 2013, **395**, 198–204.

14. M. R. Gandhi and S. Meenakshi, *Carbohyd. Polym.*, 2013, **91**, 631–637.

15. L. Tang, Y. Cai, G. D. Yang, Y. Y. Liu, G. M. Zeng, Y. Y. Zhou, S. S. Li, J. J. Wang, S. Zhang, Y. Fang and Y. B. He, *Appl. Surf. Sci.*, 2014, **314**, 746–753.

16. L. Tang, Y. Fang, Y. Pang, G. M. Zeng, J. J. Wang, Y. Y. Zhou, Y. C. Deng, G. D. Yang, Y. Cai and J. Chen, *Chem. Eng. J.*, 2014, **254**, 302–312.

17. P. Wang and I.M.C. Lo, *Water Res.*, 2009, **43**, 3727–3734.

18. L. J. Xu and J. L. Wang, *Environ. Sci. Technol.*, 2012, **46**, 10145–10153.

19. X. Guo, G. T. Fei, H. Su and L. D. Zhang, *J. Phys. Chem. C*, 2011, **115**, 1608–1613.

20. Y. Yang, M. H. Diao, M. M. Gao, X. F. Sun, X. W. Liu, G. H. Zhang, Z. Qi and S. G. Wang, *Electrochim. Acta*, 2014, **132**, 496–503.

21. D. Y. Zhao, J. L. Feng, Q. S. Huo, N. G. Melosh, H. Fredrickson, B. F. Chmelka and G. D. Stucky, *Science*, 1998, **279**, 548–552.

22. X. F. Wang, P. Liu, Y. Tian and L. Q. Zang, *Micropor. Mesopor. Mat.*, 2011,**145**, 98–103.

23. Z. B. Lei, X. X. Sun, H. J. Wang, Z. H. Liu, and X. S. Zhao, *ACS Appl. Mater. Inter.*, 2013, **5**, 7501–7508.

24. B. Yuan, X. F. Wu, Y. X. Chen, J. H. Huang, H. M. Luo and S. G. Deng, *Environ. Sci. Technol.*, 2013, **47**, 5474−5480.

493 25. W. Teng, Z. X. Wu, D. Feng, J. W. Fan, J. X. Wang, H. Wei, M. J. Song and D.
494 Y. Zhao, *Environ. Sci. Technol.*, 2013, **47**, 8633−8641.
495 26. J. Yang, J. X. Wu, Q. F. Lü and T. T. Lin, *ACS Sustainable Chem. Eng.*, 2014, **2**,
496 1203−1211.
497 27. G. D. Yang, L. Tang, X. X. Lei, G. M. Zeng, Y. Cai, X. Wei, Y. Y. Zhou, S. S. Li,
498 Y. Fang and Y. Zhang, *Appl. Surf. Sci.*, 2014, **292**, 710−716.
499 28. J. H. Zhu, S. Y. Wei, H. B. Gu, S. B. Rapole, Q. Wang, Z. P. Luo, N.
500 Haldolaarachchige, D. P. Young and Z. H. Guo, *Environ. Sci. Technol.*, 2012,
501 **46**, 977−985.
502 29. G. X. Yang and H. Jiang, *Water Res.*, 2014, **48**, 396−405.
503 30. Y. Li, S. M. Zhu, Q. L. Liu, Z. X. Chen, J. J. Gu, C. L. Zhu, T. Lu, D. Zhang and
504 J. Ma, *Water Res.*, 2013, **47**, 4188−4197.
505 31. Y. J. Lia, B. Y. Gao, T. Wu, D. J. Sun, X. Li, B. Wang and F. J. Lu, *Water Res.*,
506 2009, **43**, 3067−3075.
507 32. Z. H. Ai, Y. Cheng, L. Z. Zhang and J. R. Qiu, *Environ. Sci. Technol.*, 2008, **42**,
508 6955–6960.
509 33. Y. Pang, G. M. Zeng, L. Tang, Y. Zhang, Y. Y. Liu, X. X. Lei, Z. Li, J. C. Zhang,
510 Z. F. Liu and Y. Q. Xiong, *Chem. Eng. J.*, 2011, 175, 222–227.
511 34. A. G. Yavuz, E. Dincturk-Atalay, A. Uygun, F. Gode and E. Aslan, *Desalination*,
512 2011, **279**, 325–331.
513 35. V. K. Gupta, D. Pathania, S. Sharma and P. *J.* Singh, *Colloid Interf. Sci.*, 2013,
514 **401**, 125−132.

36. M. Anbia, K. Kargosha and S. Khoshbooei, *Chem. Eng. Res. Des.*, 2014, DOI: 10.1016/j.cherd.2014.07.018.

37. W. Q. Cai, L. J. Tan, J. G. Yu, M. Jaroniec, X. Q. Liu, B. Cheng and F. Verpoort, *Chem. Eng. J.*, 2014, **239**, 207–215

38. J. Zhu, H. Gu, J. Guo, M. Chen, H. Wei, Z. Luo, H. A. Colorado, N. Yerra, D. Ding, T. C. Ho, N. Haldolaarachchige, J. Hopper, D. P. Young, Z. Guo, S. Wei, *J. Mater. Chem. A*, 2014, **2**, 2256–2265.

39. E. Petala, K. Dimos, A. Douvalis, T. Bakas, J. Tucek, R. Zbořil, M. A. Karakassides, *J. Hazard. Mater.*, 2013, **261**, 295–306.

40. L. N. Shi, X. Zhang and Z. L. Chen, *Water Res.*, 2011, **45**, 886–892.

41. O. Hakami, Y. Zhang and C. J. Banks, *Water Res.*, 2012, **46**, 3913−3922.

42. P. L. Younger, Blackwell Publishing Ltd., Main Street, Malden, MA, USA, 2007.

43. J. K. Yang and S. M. Lee, *Chemosphere*, 2006, **63**, 1677−1684.

44. W. T. Yu, L. Y. Zhang, H. Y. Wang and L. Y. Chai, *J. Hazard. Mater.*, 2013, **260**, 789–795.

45. J. Wang, K. K. Zhang and L. Zhao, *Chem. Eng. J.*, 2014. **239**, 123−131.

46. Y. Zhang, Q. Li, L. Sun, R. Tang and J. P. Zhai, *J. Hazard. Mater.*, 2010, **175**, 404−409.

47. Z. X. Wu, W. Li, P. A. Webley and D. Y. Zhao, *Adv. Mater.*, 2012, **24**, 485–491.

535 **Table captions**

536 **Table 1** Adsorption kinetic model parameters for the adsorption of Cr(VI) onto three
537 different mesoporous adsorbents.

538 **Table 2** Langmuir and Freundlich isotherm parameters for the adsorption of Cr(VI)
539 onto PANI−Fe/OMC at different pH values and temperatures.

540 **Table 3** Comparison of Cr(VI) uptake capacity of various adsorbents.

541 **Table 4** Thermodynamic parameters for the adsorption of Cr(VI) onto
542 PANI−Fe/OMC at different temperatures.

543

544 **Figure captions**

545 **Fig. 1.** TEM images of as−synthesized SBA−15 (a, b) and PANI–Fe/OMC (c, d).

546 **Fig. 2.** FTIR spectra of SBA−15 (a), Fe/OMC (b), and PANI–Fe/OMC (c).

547 **Fig. 3.** Kinetics of Cr(VI) adsorption onto the PANI–Fe/OMC (a), where the inset is
548 the pseudo second–order model for Cr(VI) adsorption; UV–vis absorption of the
549 solutions after treated with PANI−Fe/OMC as a function of contact time (b). Initial
550 Cr(VI) concentration = 80 mg/L; pH = 5.0; T = 298 K.

551 **Fig. 4.** The isotherms of Cr(VI) adsorption onto PANI−Fe/OMC at different pH
552 values (a) and temperatures (b).

553 **Fig. 5.** The effect of co−existing anions on Cr(VI) adsorption and the inset is the
554 effect of organic matters.

555 **Fig. 6.** Comparison of dynamic profile curves of Cr(VI) uptake onto SBA−15,
556 Fe/OMC and PANI−Fe/OMC (a) and ultrapure water, tap water and river water (b).

557 **Fig. 7.** FTIR spectrum of PANI−Fe/OMC before (a) and after (b) contact with Cr(VI).

558 **Fig. 8.** XPS spectra of Cr 2p for PANI–Fe/OMC interact with Cr(VI) (a, b). N 1s and
559 O1s for the PANI−Fe/OMC before (c, e) and after Cr(VI) adsorption (d, f).

560 **Fig. 9.** Schematic for the adsorption–couple reduction mechanisms behind removal of
561 Cr(VI) by PANI-Fe/OMC.

562

Table 1 Adsorption kinetic model parameters for the adsorption of Cr(VI) onto three different mesoporous adsorbents.

Adsorbents	Pseudo-first-order model			Pseudo-second-order model			
	k_1 (min^{-1})	$q_{e,cal}$ (mg/g)	R^2	k_2 (g/mg/min)	$q_{e,cal}$ (mg/g)	R^2	$q_{e,exp}$ (mg/g)
SBA-15	0.154	6.18	0.859	0.0189	7.20	0.997	7.04
Fe/OMC	0.177	39.86	0.945	0.0047	44.13	0.999	43.02
PANI-Fe/OMC	0.351	68.58	0.938	0.0046	74.96	0.999	74.38

Table 2 Langmuir and Freundlich isotherm parameters for the adsorption of Cr(VI) onto PANI-Fe/OMC at different pH values and temperatures.

Conditions		Langmuir			Freundlich		
		K_L (L/mg)	q_{max} (mg/g)	R^2	K_F	n	R^2
pH values	pH 2.0	0.120	172.33	0.988	46.45	4.08	0.935
	pH 5.0	0.065	132.15	0.995	47.30	5.65	0.857
	pH 7.0	0.058	104.27	0.994	36.14	5.56	0.859
	pH 9.0	0.051	79.18	0.998	26.25	5.41	0.863
Temperatures	293 K	0.134	151.60	0.994	44.66	4.42	0.897
	303 K	0.165	180.04	0.986	53.87	4.36	0.919
	313 K	0.176	204.56	0.988	62.18	4.38	0.913

Table 3 Comparison of Cr(VI) uptake capacity of various adsorbents.

Adsorbent	Q_m (mg/g)	Equilibrium time (min)	pH	T (K)	References
Polyaniline coated ethyl cellulose	38.76	30	1.0	303	[19]
N–doped porous carbon with magnetic particles	30.96	30	3.0	298	[30]
Aluminum magnesium mixed hydroxide nanoparticles	112.00	150	4.0	313	[31]
Fe@Fe_2O_3 core-shell nanowires	7.78	300	6.4	298	[32]
PEI-modified magnetic adsorbent	78.13	30	2.0	298	[33]
Poly(2-ethylaniline)/ chitosan	147.16	240	3.0	298	[34]
Ficus carica fiber based activated carbon	44.84	105	3.0	303	[35]
Modified magnetic mesoporous silica MCM-48	115.60	90	4.0	298	[36]
Amino-functionalized mesoporous alumina	59.50	60	2.0	298	[37]
Mesoporous magnetic carbon nanocomposite	3.74	10	/	298	[38]
PANI–Fe/OMC	172.33	120	2.0	298	This study

Table 4 Thermodynamic parameters for the adsorption of Cr(VI) onto PANI-Fe/OMC at different temperatures.

Temperatures	K_L (L/mol)	ΔS^0 (J/K/mol)	ΔH^0 (kJ/mol)	ΔG^0 (kJ/mol)
293 K	6968			-2.16
303 K	8580	109.42	10.45	-2.27
313 K	9152			-2.38

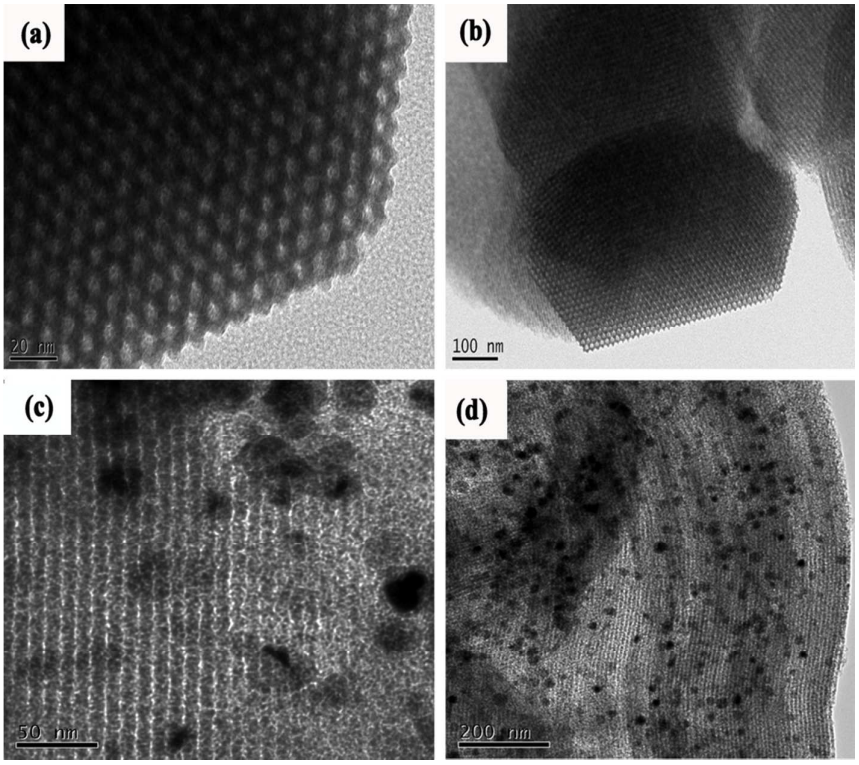

Fig. 1.

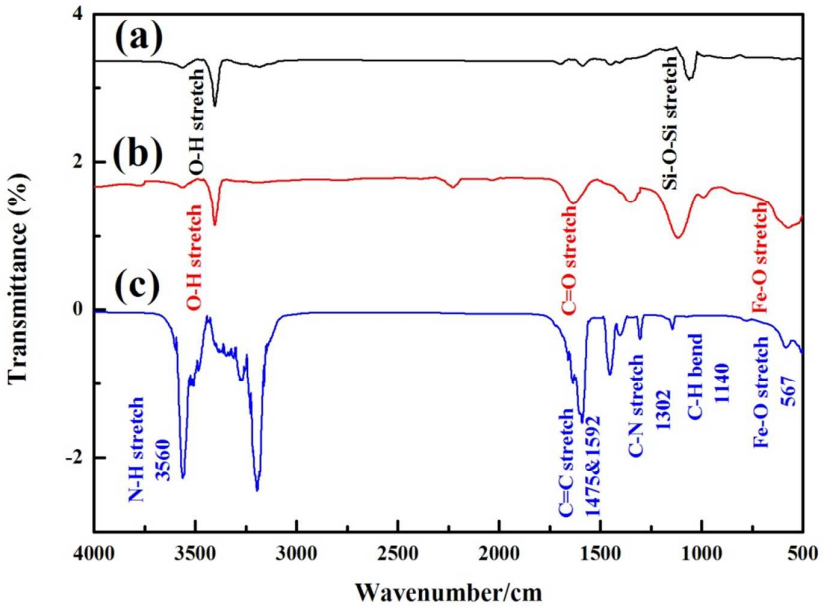

Fig. 2.

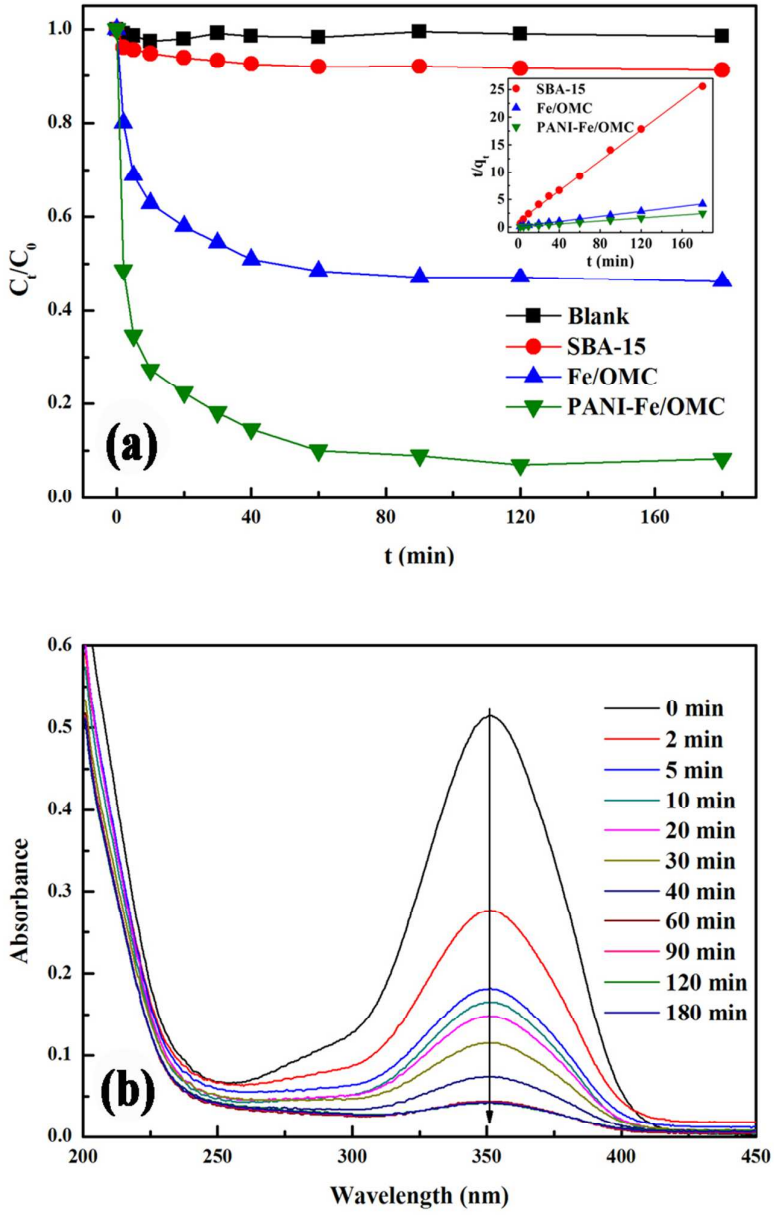

Fig. 3.

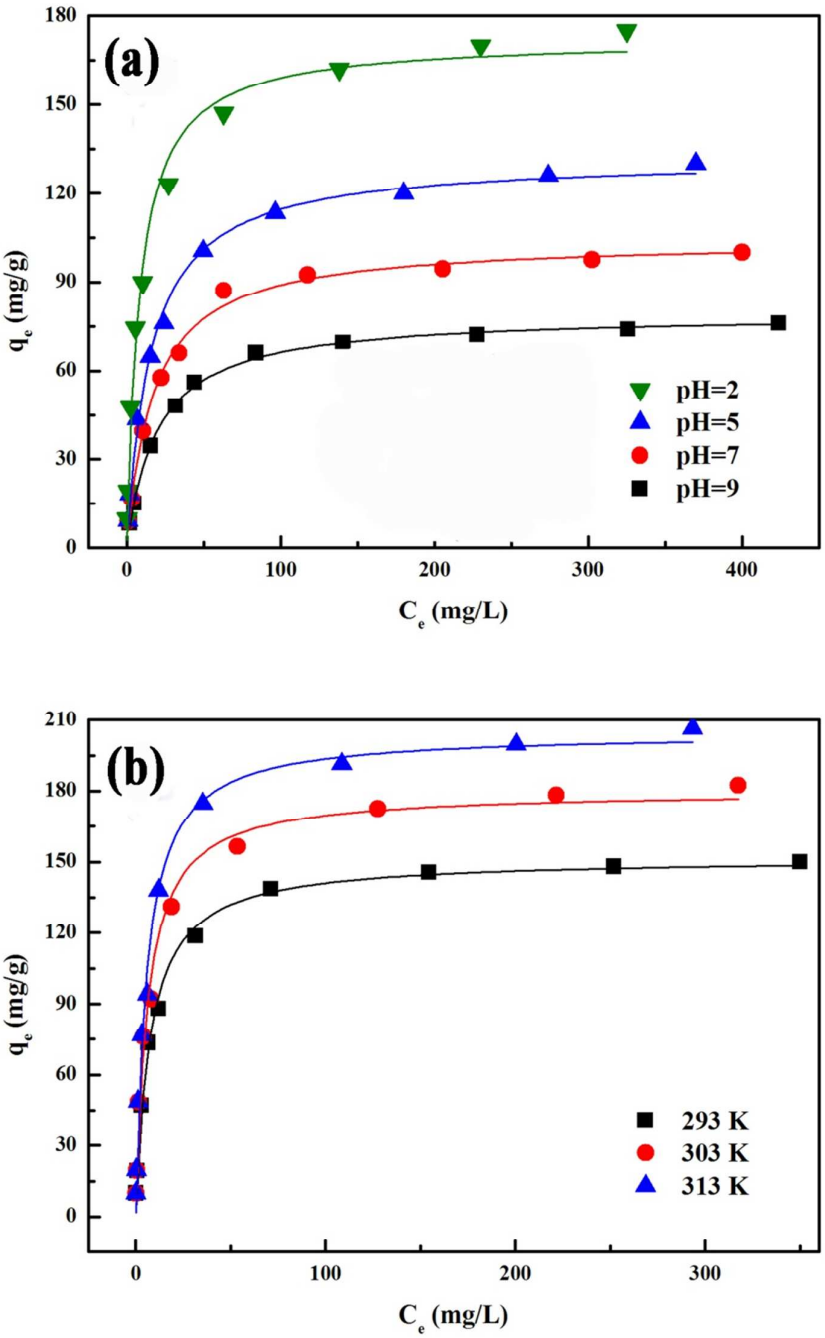

Fig. 4.

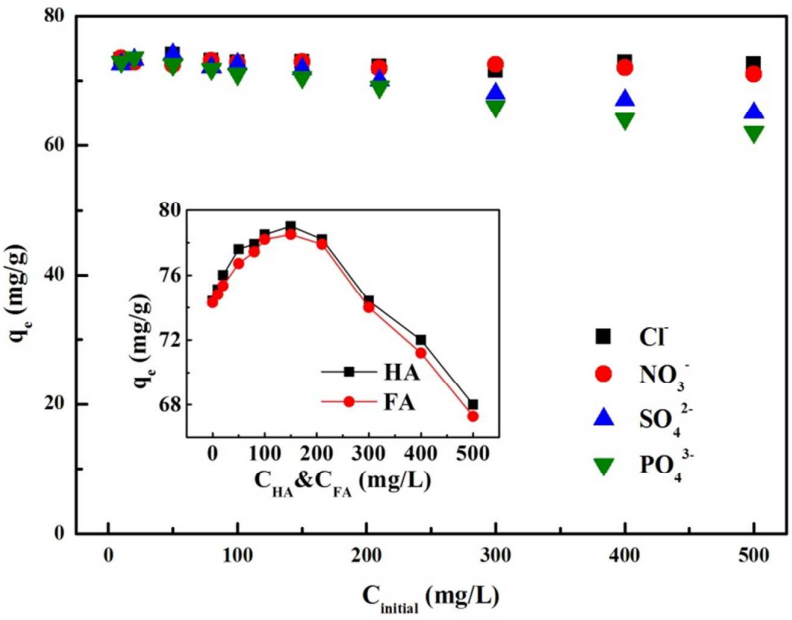

Fig. 5.

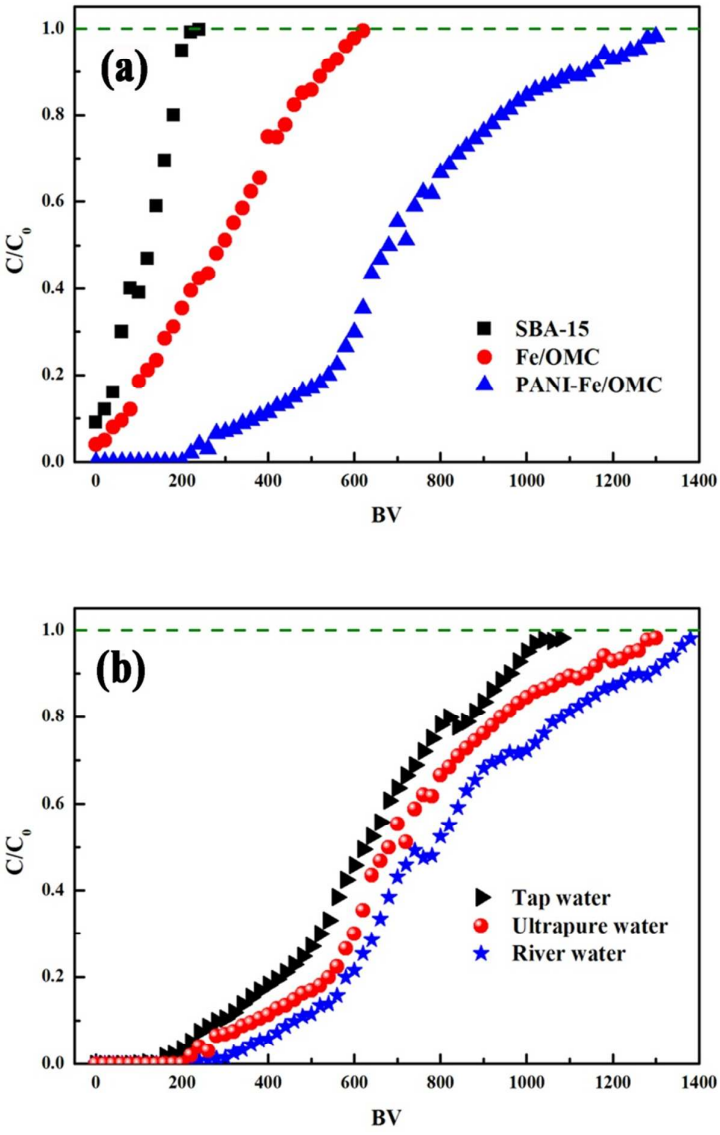

Fig. 6.

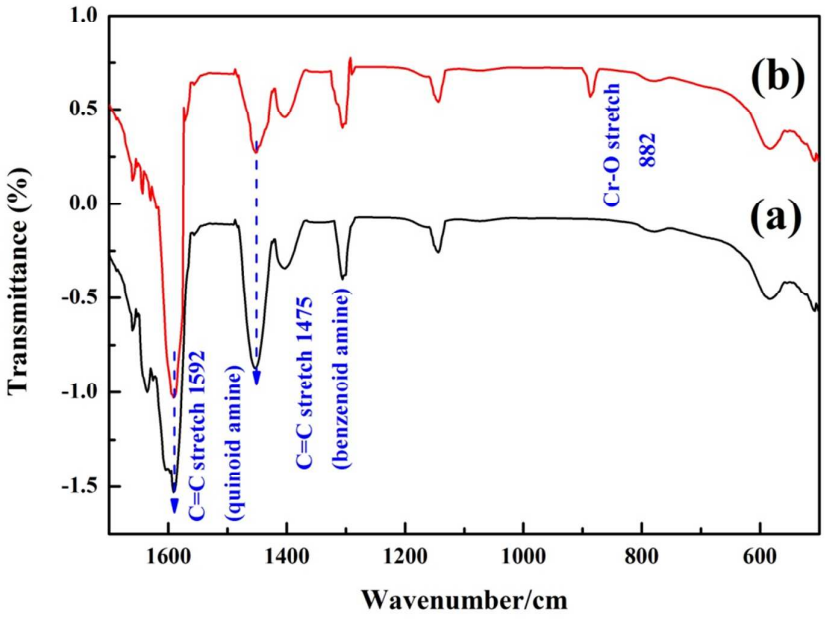

Fig. 7.

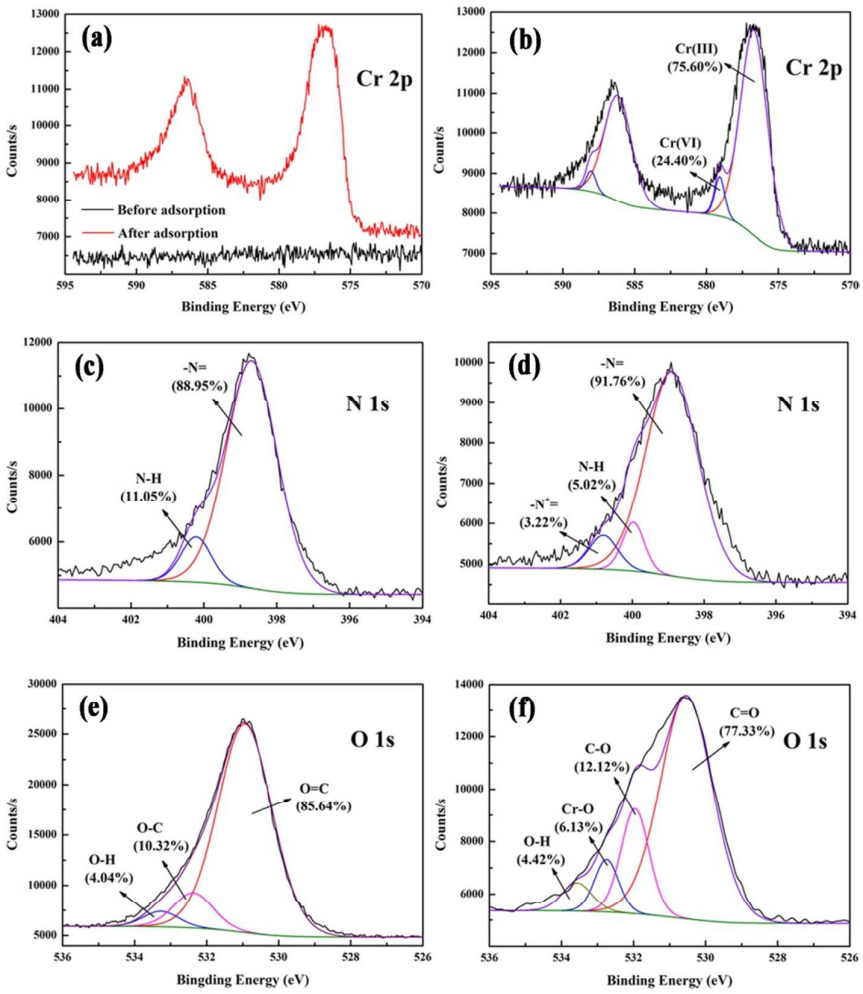

Fig. 8.

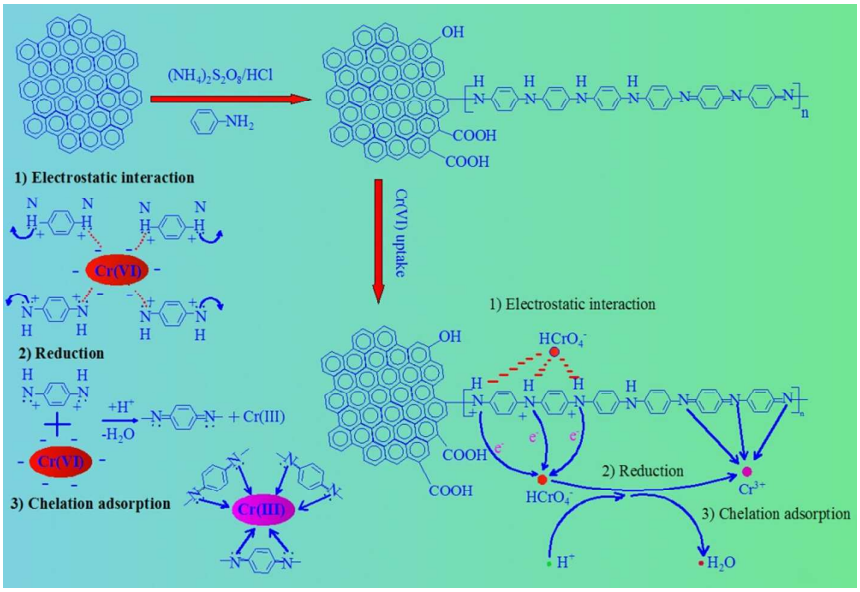

Fig. 9.